

An experimental investigation on intra-fractional organ motion effects in lung IMRT treatments

Steve B Jiang, Cynthia Pope, Khaled M Al Jarrah, Jong H Kung,
Thomas Bortfeld and George T Y Chen

Department of Radiation Oncology, Massachusetts General Hospital and Harvard Medical School, Boston, MA 02114, USA

E-mail: jiang.steve@mgh.harvard.edu

Received 24 February 2003

Published 3 June 2003

Online at stacks.iop.org/PMB/48/1773

Abstract

Respiration-induced tumour motion can potentially compromise the use of intensity-modulated radiotherapy (IMRT) as a dose escalation tool for lung tumour treatment. We have experimentally investigated the intra-fractional organ motion effects in lung IMRT treatments delivered by multi-leaf collimator (MLC). An in-house made motor-driven platform, which moves sinusoidally with an amplitude of 1 cm and a period of 4 s, was used to mimic tumour motion. Tumour motion was simulated along cranial-caudal direction while MLC leaves moved across the patient from left to right, as in most clinical cases. The dose to a point near the centre of the tumour mass was measured according to geometric and dosimetric parameters from two five-field lung IMRT plans. For each field, measurement was done for two dose rates (300 and 500 MU min⁻¹), three MLC delivery modes (sliding window, step-and-shoot with 10 and 20 intensity levels) and eight equally spaced starting phases of tumour motion. The dose to the measurement point delivered from all five fields was derived for both a single fraction and 30 fractions by randomly sampling from measured dose values of each field at different initial phases. It was found that the mean dose to a moving tumour differs slightly (<2–3%) from that to a static tumour. The variation in breathing phase at the start of dose delivery results in a maximum variation around the mean dose of greater than 30% for one field. The full width at half maximum for the probability distribution of the point dose is up to 8% for all five fields in a single fraction, but less than 1–2% after 30 fractions. In general, lower dose rate can reduce the motion-caused dose variation and therefore might be preferable for lung IMRT when no motion mitigation techniques are used. From the two IMRT cases we studied where tumour motion is perpendicular to MLC leaf motion, the dose variation was found to be insensitive to the MLC delivery mode.

(Some figures in this article are in colour only in the electronic version)

1. Introduction

Local failure is a major cause of tumour-related death in locally advanced non-small-cell lung cancer. Dose escalation holds the promise of increasing local tumour control and survival (Choi and Doucette 1981, Mehta *et al* 2001). Highly conformal radiotherapy techniques, such as intensity-modulated radiotherapy (IMRT), will be necessary to achieve significant dose escalation without unacceptable lung and oesophageal morbidity (Marnitz *et al* 2002).

IMRT has been shown to be a useful modality to escalate target dose and/or to spare more adjacent normal tissues for many tumour sites (Intensity Modulated Radiation Therapy Collaborative Working Group 2001). However, respiration-induced intra-fractional tumour motion may potentially compromise the application of IMRT to lung tumours. Large safety margins are needed to ensure there is no geometric missing of the target. However, even if sufficient margins are applied, the target dose distribution may still be degraded due to the tumour motion.

There are two types of intra-fractional organ motion effects. One is due to the non-uniform dose distribution and can be called *dose blurring effect*. Imagine a point inside the target moving sinusoidally in a dose grid. The cumulative dose to the point is the average over the moving range, which differs from the dose when the point is static if dose inhomogeneity exists in the neighbouring area. For a point near the target edge, this effect is significant (i.e., geometric miss) but can be eliminated by using a larger margin. For a point deep inside the target, this effect can often be ignored because usually (1) the composite dose distribution from all treatment fields is relatively uniform inside the target, and (2) the dose delivery time for a single field is much longer than the period of patient's breathing cycle. This type of organ motion effect does not depend on treatment delivery techniques, which means it also exists in statically delivered treatments (such as physical compensator-based IMRT). The other organ motion effect may be called *interplay effect* and is unique to dynamical delivery techniques, e.g., using multi-leaf collimator (MLC) (Yang *et al* 1997, Yu *et al* 1998, Pemler *et al* 2001, Bortfeld *et al* 2002). This effect is caused by the interplay between the motion of the target and the motion of the radiation beam defined by, e.g., MLC aperture. It exists even when one tries to deliver a uniform dose distribution with MLC.

In order to treat lung tumours with IMRT, the intra-fractional tumour motion effect should be carefully studied. Even when various motion mitigation techniques, such as respiratory gating, are used, the study of the motion effect on the target dose is still necessary, since we need to answer questions such as: for the residual motion, how small is small enough?

Yang *et al* (1997) measured the interplay effect in tomotherapy delivered with both continuous helical beam and sequential rotational beam, using a computer-controlled dynamic phantom to simulate tomotherapy dose delivery and longitudinal tumour motion. For MLC-based IMRT, the interplay effect on the delivery of a single field was numerically simulated using a simple analytical model by Yu *et al* (1998). Conclusions have been drawn about the dependence of the effect (1) on the relative speed of tumour motion and MLC leaf motion, and (2) on the relative width of leaf gap and the tumour motion amplitude (Yu *et al* 1998). The interplay effect has also been studied in treatments using enhanced dynamic wedges (EDW) by Pemler *et al* (2001). The magnitude of the effect on the delivered dose distributions was studied for a variety of factors, including wedge angle, amplitude of organ motion, respiratory rate, asymmetry of the respiratory cycle, beam energy and the dose rate (Pemler *et al* 2001).

The studies of Yu *et al* (1998) and Pemler *et al* (2001) have dealt with two widely used treatment modalities (IMRT and EDW). However, those two numerical studies only considered a single field and more importantly, scenarios where MLC leaves or linac jaws

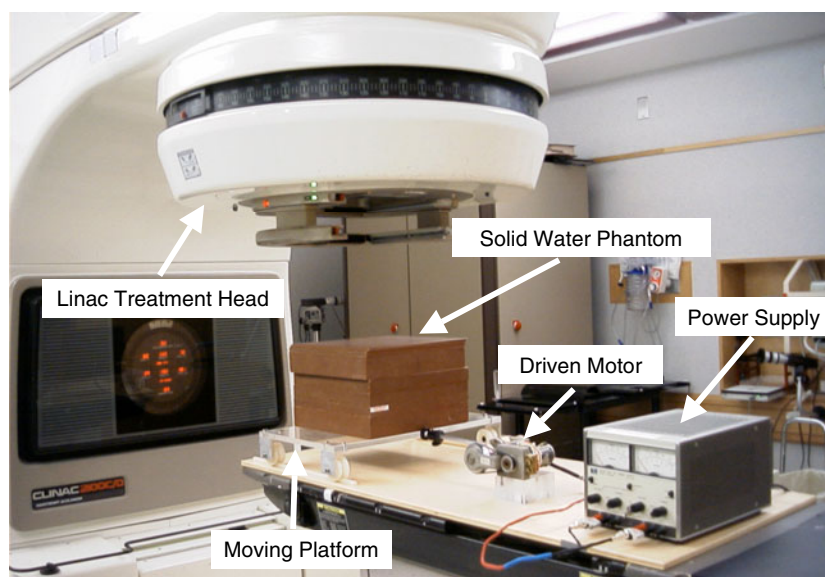


Figure 1. An in-house made motor-driven moving phantom for tumour motion simulation.

move along the tumour motion direction. In many clinical lung IMRT cases, tumour moves along cranial-caudal direction while MLC leaves move along left–right direction.

The mechanism of the interplay effect is totally different when the angle between tumour motion and MLC motion is 0° or 90° . When tumour motion is parallel to the leaf motion, the magnitude of the effect is determined by the interplay between the tumour and one leaf pair. When tumour motion is perpendicular to the leaf motion, what causes the effect is the interplay between the tumour and the unaligned neighbouring leaf end positions. Therefore, the conclusions drawn by Yu *et al* (1998) and Pehler *et al* (2001) may not be applicable to the cases where tumour motion is normal to the MLC leaf motion.

Intuitively, when tumour motion is perpendicular to leaf motion, it will not cause any problem as long as the neighbouring leaf ends are aligned along the tumour trajectory. However, in a realistic IMRT case, it is generally impossible to keep the same neighbouring leaf end positions throughout the whole leaf sequence. Therefore, in reality, the interplay effect cannot be ignored when tumour motion is normal to leaf motion, and it is clinically relevant to find out the magnitude of the effect.

Recently, we have investigated the intra-fractional organ motion effect using statistical analysis and computer simulation methods (Bortfeld *et al* 2002). The current paper presents an experimental study on the magnitude of the effect in lung IMRT treatments where tumour motion is perpendicular to MLC leaf motion, as well as its dependence on the delivery mode, dose rate and motion starting phase.

2. Method and materials

An in-house developed motor-driven moving platform was used in this study to simulate the tumour motion (see figure 1). The platform is driven by a motor and able to perform one-dimensional sinusoidal movement on rails. The amplitude of the movement is fixed to be 2 cm, peak-to-peak. The period can be easily changed by adjusting the output voltage of a

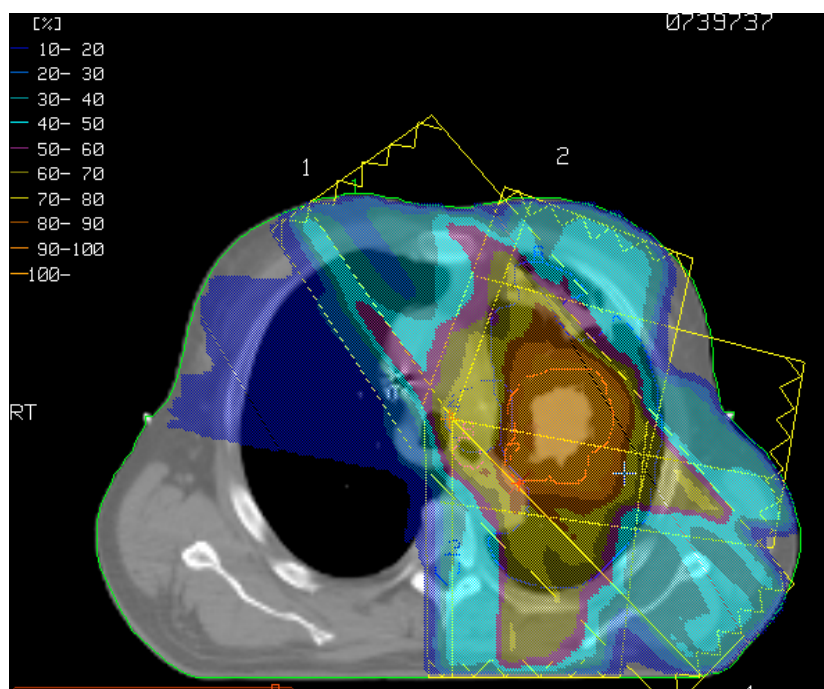


Figure 2. An axial CT slice and the dose distribution from the IMRT plan used in the measurement for patient A. The contour in red denotes the planning target volume. The measurement point was chosen to be near the centre of the tumour mass.

24V DC power supply. Proper amount of solid water was placed on the platform for dosimetric measurement. For all the measurements done in this study, the motion period was kept in the range from 3.5 to 4 s, which is close to the breathing cycle period of an average patient (Ozhasoglu and Murphy 2002, Seppenwoolde *et al* 2002, Neicu *et al* 2003).

Actual IMRT plans for two lung cancer patients (patient A and patient B) were used in the measurement. Plans were optimized by the Helios inverse planning system V2.7 (Varian Medical Systems, Inc., Palo Alto, CA, USA). Each plan has five fields, and the monitor units (MU) for each field range from about 150 to 420. Figure 2 shows an axial CT slice and the overlaid dose distribution from the IMRT plan used in the measurement for patient A. We can see that the tumour mass in patient A was well defined. The tumour location and size for patient B are similar.

The measurement point was located near the centre of the tumour mass for both patients. A 0.6 cc farmer chamber was placed in solid water phantom on the top of the moving platform. The linac gantry was always at 0° (IEC) no matter which IMRT field was being measured. However, the solid water phantom and the ion chamber were set up using parameters (such as source-to-surface distance (SSD), off-axis distance, effective depth) from the plan. Therefore, for each field, the chamber position corresponded to the same point in the plan near the tumour centre.

Measurements were performed on a Varian 2100C linear accelerator, equipped with an MLC of 26 leaf pairs (Varian Medical Systems, Inc., Palo Alto, CA, USA). The leaf width projected at the isocentre level is 1 cm. MLC leaf sequence files and MUs for all fields were obtained from the planning system. The phantom moved along the patient's long axis while

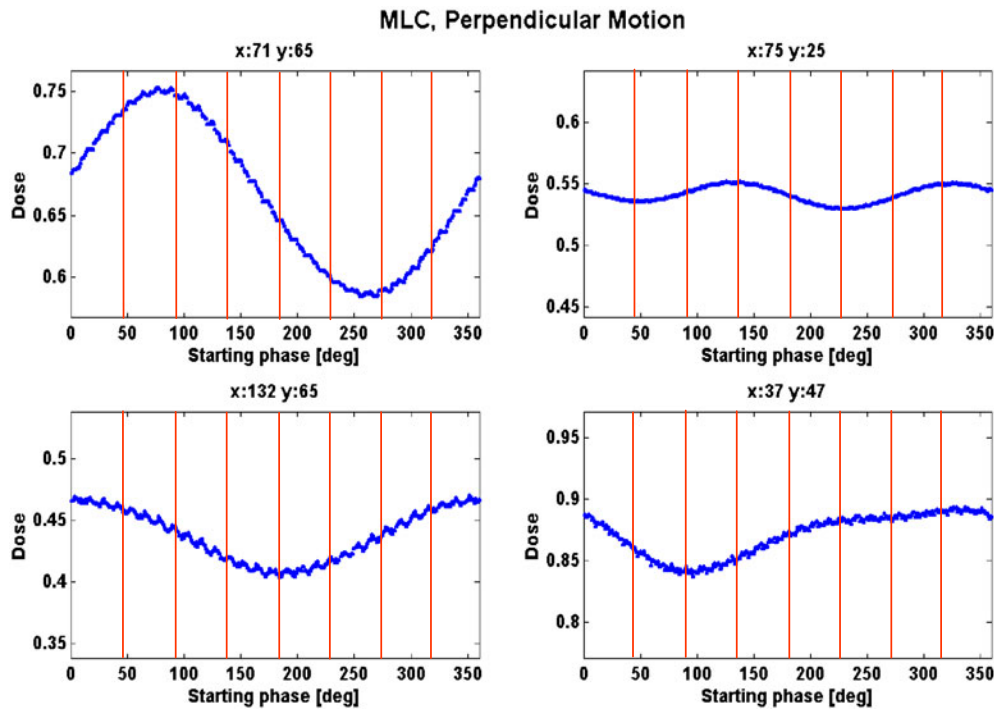


Figure 3. Simulated dose to a moving point from an IMRT field as a function of the motion phase of the point when treatment starts. Dose values are normalized arbitrarily. Points move in a sinusoidal way, perpendicular to the MLC leaf motion. The four points are located in areas with representative dose gradient distributions (see Bortfeld *et al* (2002) for details). Vertical lines indicate the eight initial phases used in the current measurement.

MLC leaves moved across the patient from left to right. Therefore the two motions are always perpendicular to each other in this study. For each field, the measurement was made for two dose rates (300 and 500 MU min⁻¹), and three MLC delivery modes: (1) sliding window (SW), (2) step-and-shoot with 10 (SS10) and (3) 20 intensity levels (SS20).

The dose delivered to a point in a moving target from the j th field ($j = 1, 2, \dots, 5$), $d^{(j)}$, depends on the initial phase of the motion when the treatment starts, φ , i.e., $d^{(j)} = d^{(j)}(\varphi)$ (Bortfeld *et al* 2002). To estimate the dose variation caused by different initial phases, the measurements were repeated for eight initial phases ($\varphi_i = i\pi/4$, $i = 1, 2, \dots, 8$). Each initial phase was visually determined based on the position of a marker on the driven gear of the motor, through a video monitoring system. Therefore, the spread of the eight initial phases in the breathing cycle is only approximately equal.

To understand how well the dose measured at eight phases, i.e., $d_i^{(j)} = d^{(j)}(\varphi_i)$, $i = 1, 2, \dots, 8$, represents the function $d^{(j)} = d^{(j)}(\varphi)$, we calculated the function for points at four different locations in one field (Bortfeld *et al* 2002). The locations represent four typical dose gradient situations: low dose gradient, high dose gradient in either one of the principal directions or both directions. As shown in figure 3, the function $d^{(j)} = d^{(j)}(\varphi)$ is smooth. Therefore, $d_i^{(j)}$ ($i \in [1, 8]$) is a good representative of the function, and any inaccuracy in starting the measurement at one of the eight initial phases should not significantly affect the measured dose values.

As we have known from our previous work (Bortfeld *et al* 2002), the probability distribution of the dose to a moving point from one field can be approximated as

$$f(d_i^{(j)}) = \frac{1}{\pi} \frac{1}{\sqrt{W^2 - (d_i^{(j)} - \bar{d})^2}} \quad (1)$$

where \bar{d} is the mean dose and W is the possible maximum variation of the dose value from the mean. Equation (1) holds when the target point moves in a sinusoidal way and the dose gradient in the neighbouring region is linear. The distribution has two sharp peaks when $|d_i^{(j)} - \bar{d}| \rightarrow W$. Parameters W and \bar{d} can be used to characterize the distribution and an approximation of them can be derived using the measured values of $d_i^{(j)}$ ($i \in [1, 8]$).

For the real patient treatment, the phase of the tumour motion at the beginning of each field delivery is usually unknown. Therefore, the dose from all fields in one treatment fraction is the summation of the dose from each field at a random initial phase. The dose to the measurement point from all fields in one fraction can be calculated using the measured single field dose:

$$D_1 = \sum_{j=1}^5 d_{\zeta}^{(j)}. \quad (2)$$

Here, ζ is a random integer number and $\zeta \in [1, 8]$. Similarly, we can also calculate the dose to the measurement point after 30 fractions of treatment:

$$D_{30} = \sum_{k=1}^{30} \sum_{j=1}^5 d_{\zeta}^{(j)}. \quad (3)$$

The simulation based on equations (2) and (3) was performed 10^5 times. The statistical uncertainties associated with the resulting probability distributions of D_1 and D_{30} are negligible.

The dose to the measurement point was also measured for every dose rate/delivery mode combination when the phantom is static. The measured static dose values were used to normalize the dose values to the moving point.

3. Results

In tables 1 and 2, we present the mean (\bar{d} in equation (1)) and maximum variation ($2W$ in equation (1)) of the measured dose values for each IMRT field at eight different initial phases for patients A and B, for three delivery modes (SW, SS10, SS20) and two dose rates (300 and 500 MU min⁻¹). All values are normalized to the corresponding static dose values. The delivery time for each field is also given. The mean dose from one field only differs by a few per cent from the corresponding static dose, while the maximum dose variation can be up to 30% of the static dose.

The probability distributions of the dose to the measurement point from all IMRT fields after one fraction or 30 fractions, calculated from the measured single field dose values, are shown in figures 4 and 5, for patients A and B, respectively. The curves are plotted for different dose rate/delivery mode combinations: solid lines—300 MU min⁻¹, dashed lines—500 MU min⁻¹; panels (a) and (b)—sliding window; panels (c) and (d)—step-and-shoot with 10 intensity levels and panels (e) and (f)—step-and-shoot with 20 intensity levels. It can be seen that the distributions for 30 fractions are much narrower than those for one fraction. In general, the distributions for the 500 MU min⁻¹ dose rate are wider than those for the

Table 1. Mean value and maximum variation of the measured doses (normalized to the corresponding static dose value) to the measurement point from each IMRT field at eight different initial phases for patient A, for three delivery modes (sliding window: SW; step-and-shoot with 10 intensity levels: SS10; and step-and-shoot with 20 intensity levels: SS20) and two dose rates (300 and 500 MU min⁻¹). The delivery time for each field is also given.

Field no	Delivery mode	Delivery time (s)		Mean dose (%)		Max. variation (%)	
		300 MU min ⁻¹	500 MU min ⁻¹	300 MU min ⁻¹	500 MU min ⁻¹	300 MU min ⁻¹	500 MU min ⁻¹
1	SW	45	31	100.3	99.9	2.1	6.4
	SS10	48	34	103.3	102.3	3.9	8.0
	SS20	48	36	103.4	101.6	4.7	5.9
2	SW	87	53	104.9	104.1	2.2	7.7
	SS10	83	58	103.1	103.3	4.7	8.4
	SS20	84	57	105.5	105.5	9.0	9.8
3	SW	47	30	101.5	101.8	2.3	4.4
	SS10	40	29	103.3	102.3	6.8	7.9
	SS20	41	31	103.1	102.3	3.6	5.6
4	SW	53	34	102.9	101.7	2.4	11.7
	SS10	52	36	100.6	102.6	6.8	4.9
	SS20	55	39	101.1	101.2	1.7	5.6
5	SW	58	38	100.6	100.5	3.9	4.5
	SS10	61	41	101.6	101.0	9.2	4.2
	SS20	63	45	101.4	100.7	2.1	2.1

Table 2. Same as table 1, but for patient B.

Field no	Delivery mode	Delivery time (s)		Mean dose (%)		Max. variation (%)	
		300 MU min ⁻¹	500 MU min ⁻¹	300 MU min ⁻¹	500 MU min ⁻¹	300 MU min ⁻¹	500 MU min ⁻¹
1	SW	87	55	103.8	102.7	5.3	8.0
	SS10	82	56	94.3	93.6	6.7	8.4
	SS20	86	59	101.6	100.4	22.5	22.6
2	SW	63	40	101.8	101.2	5.7	6.3
	SS10	59	39	100.7	100.5	7.8	27.3
	SS20	60	43	101.7	100.0	6.9	6.7
3	SW	39	28	98.6	99.0	6.0	5.5
	SS10	35	25	97.4	98.1	2.8	7.9
	SS20	38	28	98.9	99.3	6.1	4.4
4	SW	77	48	99.1	98.1	1.5	4.8
	SS10	71	49	104.6	99.9	12.2	31.3
	SS20	73	52	101.4	101.5	4.9	6.9
5	SW	85	57	101.5	100.6	2.0	1.6
	SS10	73	50	101.3	100.5	6.9	16.7
	SS20	75	52	101.2	99.8	10.8	6.3

300 MU min⁻¹, and the distributions for step-and-shoot with 10 intensity levels are wider than those for the sliding window and step-and-shoot with 20 intensity levels.

4. Discussion

The dose to a moving target point varies with the initial phase (or position) of the point at the start of the dose delivery. Based on the analytical work of Bortfeld *et al* (2002), the probability

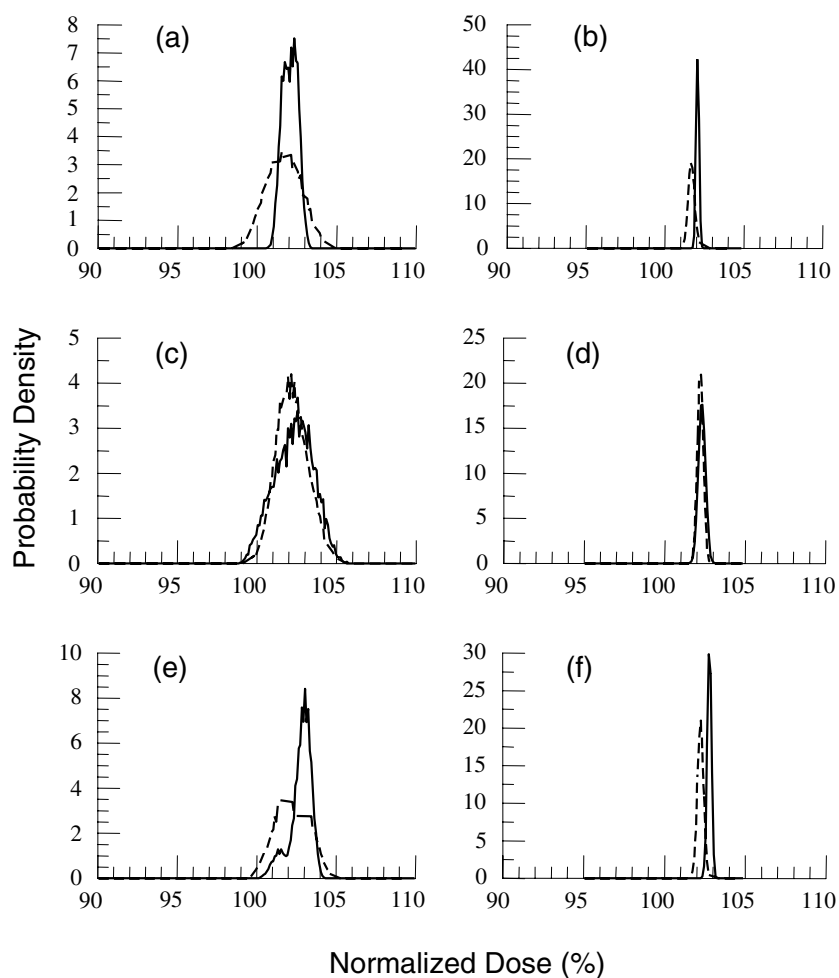


Figure 4. Probability distributions of the dose to the measurement point for patient A, for one fraction ((a), (c), (e)) and 30 fractions ((b), (d), (f)) of treatment, for three delivery modes (sliding window (a), (b); step-and-shoot with 10 intensity levels (c), (d); and step-and-shoot with 20 intensity levels (e), (f)) and two dose rates (300 (solid lines) and 500 (dashed lines) MU min^{-1}). Dose values are normalized to the corresponding dose to the measurement point when it is static.

distribution of the point dose obeys equation (1) for one field of one fraction, and has a sharp peak near either end of the distribution. When the same field is delivered for N fractions, the resulting probability distribution of the cumulative point dose is the convolution of the single fraction distribution (equation (1)) with itself for N times. Due to the central limit theorem, the multiple fraction distribution will have a Gaussian shape when N is large enough, i.e., $N \geq 5$ as found by Bortfeld *et al* (2002).

A similar rationale applies to the situation with multiple fields delivered in one fraction. As shown in figures 4 and 5 (left panels), the probability distributions of the measured point dose from all five IMRT fields, even for one fraction, have Gaussian-like shapes. After 30 fractions (right panels of figures 4 and 5), the distributions become even more Gaussian-like, and smoother and more symmetric.

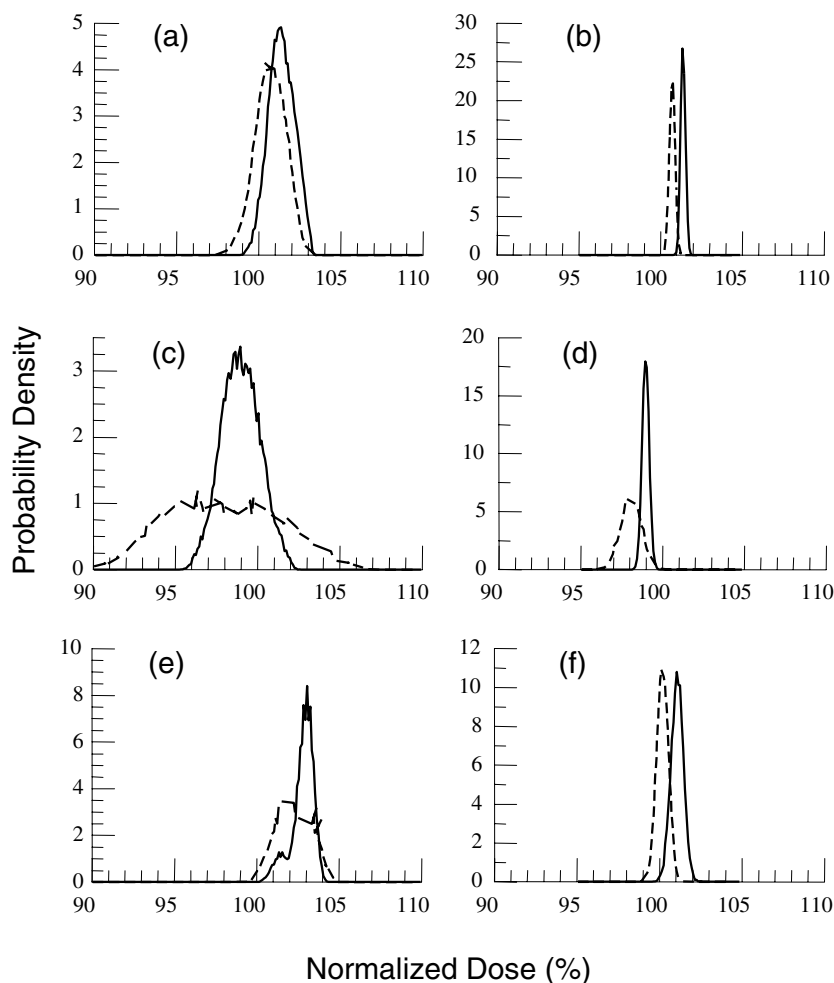


Figure 5. Same as figure 4, but for patient B.

With the increase of the number of fields and/or fractions, the width of the probability distribution decreases. For one field and one fraction, the maximum dose variations are about 12% and 30% for patients A and B, respectively. These two numbers reduce to 7% and 18% for five fields after one fraction, and 1.5% and 5% for five fields after 30 fractions. Instead of the maximum dose variation, it is more meaningful to look at the full width at half maximum (FWHM) in the case of multiple fields delivered in one fraction or 30 fractions. From figures 4 and 5, it is obvious that the distributions for 30 fractions are much narrower than those for one fraction. Considering SS10 and 500 MU min^{-1} dose rate as an example, the FWHMs are about 2.5% and 8% for one fraction, and 0.5% and 1.5% for 30 fractions, for patients A and B, respectively.

Is the observed dose variation clinically significant? The answer seems to be 'no' if we look at the dose variation after 30 fractions, which is very small (less than a couple of per cent) due to the convolution effect. However, the delivered dose can vary from fraction to fraction by up to 30% for one field (table 2) and 18% for five fields (figure 5(c)), and it is hard to simply ignore this variation of fraction size. In our previous work (Bortfeld *et al* 2002), a new

concept called equivalent uniform fraction dose was developed to evaluate the radiobiological effect of the fraction size variation. We believe a more thorough study of the radiobiological effects is necessary.

The convolution effect that reduces dose variation after multiple fractions/fields is based on the assumption that the dose delivery starts at a random initial phase for every field and every fraction, i.e., when the therapist turns on the radiation beam he/she knows nothing about patient's breathing phase. This is not true in the case of respiratory gating, in which the radiation beam is always turned on at the exact same breathing phase. The interplay between MLC motion and tumour residual motion will cause a systematical dose deviation, and this deviation will not decrease with the increase of fraction number. That is to say, potentially, the interplay effect may have more impact on gated IMRT and therefore deserves some careful investigation.

In general, smaller dose rate, i.e., longer delivery time, reduces the dose variation (see figures 4 and 5), which suggests that a slow dose rate should be used if one wants to treat a moving tumour with MLC-based IMRT and no motion mitigation techniques are used. According to Yu *et al* (1998) and Pemler *et al* (2001), the magnitude of the interplay effect is at maximum when tumour and leaf motion speeds are similar. In the current study, tumour moves from peak to peak (2 cm) in about 2 s, so the average tumour speed is approximately 1 cm s^{-1} . The MLC leaves move across the field in about 30 to 90 s (see tables 1 and 2), so the average leaf speed is in the range from 0.1 to 0.3 cm s^{-1} (assuming the field size is about 10 cm). Therefore, when the dose rate is increased, the leaf speed approaches the tumour speed and dose variation becomes larger. This is consistent with the analysis of Yu *et al* (1998) and Pemler *et al* (2001), even though their conclusion was drawn for the situation where tumour and MLC leaves move in parallel.

According to Yu *et al* (1998), dose variation generally decreases with increasing MLC leaf gap, when tumour moves along the leaf motion direction. This conclusion seems invalid when the tumour trajectory and leaf trajectory are perpendicular to each other. We may notice that in figure 4, the dose variation is about the same for all three delivery modes, and in figure 5, the step-and-shoot technique with 10 intensity levels produces an even larger dose variation than the other two delivery modes. This observation implies that the dependence of the interplay effect on the delivery mode may be totally different for situations where tumour motion is perpendicular to or in parallel with leaf motion. To understand the rationale behind the difference, further studies are necessary.

It is interesting to point out that both plans used in the study, generated by Helios inverse planning system (Varian Medical Systems, Inc., Palo Alto, CA, USA), have relatively long delivery time (ranging from 30 to 90 s per field, at 300 MU min^{-1} dose rate). Other planning systems may be able to generate plans with much less total number of MUs and thus much shorter delivery time (Chui *et al* 2001). In that case, the interplay effect may cause a much larger dose variation.

One may notice from figures 4 and 5 that the mean dose values are the same for both one fraction and 30 fractions. This is because the convolution effect only reduces the dose variation but does not change the position of the mean dose (Bortfeld *et al* 2002). In general, the mean dose value is within a couple of per cent of the static dose value. The difference between mean dose and static dose may be caused by the following factors: (1) dose blurring effect (large dose inhomogeneity around the measurement point may exist due to the application of patient plans to a phantom), and/or (2) the interplay effect. The dose inhomogeneity effect may explain the consistent peak shift shown in figures 4(b), (d) and (f). However, the dependence of the peak shift on delivery mode and dose rate, as shown in figures 5(b), (d) and (f),

can only be explained with the interplay effect. The mechanism that causes the shift in mean dose by the interplay effect is not clear and deserves further study.

An apparent weakness of the current study is that the measurements were performed only for the dose to a single point. We do not have information about other points inside the target, and more importantly, those points near the target edge where the dose blurring effect should play a big role. We plan to use film for future measurements.

We should point out that real patient breathing cycle sometimes exhibits very complicated patterns, with continuously changing amplitude and periodicity, drifting baseline (DC drifts) and the so-called envelope effect (Ozhasoglu and Murphy 2002, Seppenwoolde *et al* 2002). The tumour mean position may migrate inter- and intra-fractionally, due to the change of tidal lung volume as a function of time. Mathematically speaking, human respiration represents a non-stationary state and is very difficult to model (Ozhasoglu and Murphy 2002). Using sinusoidal oscillation to model respiratory tumour motion is just a first-order approximation. Therefore, even though we have observed that the interplay effect only introduces small target dose variation after 30 fractions, it does not guarantee a safe use of IMRT for lung cancer treatment under free breathing. It is our opinion that real-time image guidance is generally necessary for lung IMRT.

5. Conclusions

Respiration-induced intra-fractional tumour motion in MLC-delivered lung IMRT treatment causes a probability distribution for the dose to a target point, in contrast to a single dose value when the tumour is static. The mean value of the distribution (mean dose) is independent of the treatment fraction numbers and is within 2–3% to the static dose. The width of the distribution (dose variation) is caused by the difference in initial breathing phases when dose delivery starts. The maximum dose variation can be up to 30% for one field in one fraction, and 18% for all five fields after one fraction. It reduces to less than 1–2% after 30 fractions due to the convolution effect. It was found that the dose variation reduces with decreasing dose rate (increasing delivery time) and does not seem sensitive to the MLC delivery mode. Therefore, when treating a moving tumour using MLC-delivered IMRT without any motion mitigation techniques, it is recommended to use a low dose rate.

Acknowledgments

The authors would like to thank Lenny Wasileski, Dennis Mento, John Gliddon, James Wilson for building the moving platform, and Dr Ross Berbeco, Dr Greg Sharp and Dr Toni Neicu for helpful suggestions and stimulating discussions. We also want to acknowledge the constructive comments from referees. The work was supported in part by the Whitaker Foundation Grant RG-01-0175 and presented in the 44th Annual Meeting of the American Association of Physicists in Medicine, Montreal, Quebec, Canada, July 14–18 2002.

References

- Bortfeld T, Jokivarsi K, Goitein M, Kung J and Jiang S B 2002 Effects of intra-fraction motion on IMRT dose delivery: statistical analysis and simulation *Phys. Med. Biol.* **47** 2203–20
- Choi N C and Doucette J A 1981 Improved survival of patients with unresectable non-small-cell bronchogenic carcinoma by an innovated high-dose en-bloc radiotherapeutic approach *Cancer* **48** 101–9
- Chui C S, Chan M F, Yorke E, Spirou S and Ling C C 2001 Delivery of intensity-modulated radiation therapy with a conventional multileaf collimator: comparison of dynamic and segmental methods *Med. Phys.* **28** 2441–9

- Intensity Modulated Radiation Therapy Collaborative Working Group 2001 Intensity-modulated radiotherapy: current status and issues of interest *Int. J. Radiat. Oncol. Biol. Phys.* **51** 880–914
- Marnitz S, Stuschke M, Bohsung J, Moys A, Reng I, Wurm R and Budach V 2002 Intraindividual comparison of conventional three-dimensional radiotherapy and intensity modulated radiotherapy in the therapy of locally advanced non-small cell lung cancer a planning study *Strahlenther. Onkol.* **178** 651–8
- Mehta M, Scrimger R, Mackie R, Paliwal B, Chappell R and Fowler J 2001 A new approach to dose escalation in non-small-cell lung cancer *Int. J. Radiat. Oncol. Biol. Phys.* **49** 23–33
- Neicu T, Shirato H, Seppenwoolde Y and Jiang S B 2003 Synchronized moving aperture radiation therapy (SMART): average tumour trajectory for lung patients *Phys. Med. Biol.* **48** 587–98
- Ozhasoglu C and Murphy M J 2002 Issues in respiratory motion compensation during external-beam radiotherapy *Int. J. Radiat. Oncol. Biol. Phys.* **52** 1389–99
- Pemler P, Besserer J, Lombriser N, Pescia R and Schneider U 2001 Influence of respiration-induced organ motion on dose distributions in treatments using enhanced dynamic wedges *Med. Phys.* **28** 2234–40
- Seppenwoolde Y, Shirato H, Kitamura K, Shimizu S, van Herk M, Lebesque J V and Miyasaka K 2002 Precise and real-time measurement of 3D tumor motion in lung due to breathing and heartbeat, measured during radiotherapy *Int. J. Radiat. Oncol. Biol. Phys.* **53** 822–34
- Yang J N, Mackie T R, Reckwerdt P, Deasy J O and Thomadsen B R 1997 An investigation of tomotherapy beam delivery *Med. Phys.* **24** 425–36
- Yu C X, Jaffray D A and Wong J W 1998 The effects of intra-fraction organ motion on the delivery of dynamic intensity modulation *Phys. Med. Biol.* **43** 91–104